GEOLOGY | THE GEOLOGICAL SOCIETY OF AMERICA®

https://doi.org/10.1130/G46319.1

Manuscript received 29 March 2019
Revised manuscript received 28 May 2019
Manuscript accepted 29 May 2019

The role of sediment supply in the adjustment of channel sinuosity across the Amazon Basin

Joshua Ahmed[1,2]*, José Antonio Constantine[3], and Thomas Dunne[4]
[1]Energy and Environment Institute, University of Hull, Hull HU6 7RX, UK
[2]School of Earth and Ocean Sciences, Cardiff University, Cardiff CF10 3AT, UK
[3]Department of Geosciences, Williams College, Williamstown, Massachusetts 01267, USA
[4]Bren School of Environmental Science and Management, University of California, Santa Barbara, California 93106, USA

ABSTRACT

Sediment supplies are a fundamental component of alluvial river systems, but the importance of sustained supplies of externally derived sediments for the evolution of meandering planforms remains unclear. Here we demonstrate the importance of sediment supply in enhancing the growth of point bars that influence the rate of sinuosity increase through flow deflections in meander bends. We use an archive of Landsat images of 16 meandering reaches from across the Amazon Basin to show that rivers transporting larger sediment loads increase their sinuosity more rapidly than those carrying smaller loads. Sediment-rich rivers are dominated by downstream-rotating meanders that increase their sinuosity more rapidly than both extensional and upstream-rotating meanders. Downstream-rotating meanders appear to establish larger point bars that expand throughout the meander, in contrast to extensional meanders, which have smaller bars, and upstream rotating meanders, which are characterized by deposition over the bar head. These observations demonstrate that the size and position of point bars within meander bends influences flow routing and thus controls the dominant direction of meander growth. Rivers with low sediment supplies build smaller point bars, which reduces their capacity to increase meander curvature and the resulting sinuosity.

INTRODUCTION

Meandering rivers are characterized by their sinuous planforms and tendency to migrate. A range of studies have highlighted sedimentological (e.g., Schumm and Khan, 1972), biotic (e.g., Tal and Paola, 2007), valley-slope (e.g., Ouchi, 1985), and planform-curvature controls (e.g., Hickin and Nanson, 1975) on the evolution of the meandering planform, yet there remains no quantitative statement on how channel sinuosity should adjust in response to meander migration. Hooke (1984) defined patterns by which the meandering planform can adjust, but the multitude of patterns suggested that the planform response to migration is controlled by a number of variables that might prevent generalization. Schwendel et al. (2015) highlighted the sensitivity of river migration to the heterogeneity of floodplain deposits along the Beni River (Bolivia), documenting that fine-grained sediment matured in distal parts of the floodplain could affect the migration rates and forms of meanders in reaches with generally high channel mobility. Still, a formal evaluation of the nature of the relationship between meander migration and channel sinuosity has been prevented by the absence of detailed observations across a range of meandering river settings.

Meander migration is principally accomplished through curvature-driven flow divergence initiated at the bend entrance. The transverse water-surface slope facilitates sediment excavation from the bank toe, while obliquely oriented near-bed currents transport sediment inwards to the point bar (Dietrich and Smith, 1984). Point bar growth increases the length and curvature of bends, increasing the cross-stream centrifugal force (Hickin and Nanson, 1975) and enhancing cross-stream velocity by topographic steering (Dietrich and Smith, 1983; Legleiter et al., 2011). Constantine et al. (2014) observed that sediment fluxes correlated positively with rates of riverbank erosion and oxbow lake production, implying that the construction of point bars is an influence on meander migration and sinuosity adjustment. Empirical observations have documented the importance of sediment supplies in planform adjustment through bedform development (Braudrick et al., 2009; Bufe et al., 2016). In the River Ystwyth (Wales, UK), sediment supplies led to the accumulation of point-bar complexes, which intensified the development of a sinuous planform despite repeated attempts to artificially straighten the channel (Lewin, 1976). Physically based numerical models have produced similar results, with enhanced bar migration and riverbank erosion predicted along reaches that experience increased bar construction (e.g., Dunne et al., 2010; Schuurman et al., 2016). Because point bars exert a strong control on bank erosion—which determines how sinuosity changes—and rely upon sediment supply for their growth, we assess the relationship between meander migration and channel lengthening, and quantify how they vary with sediment supply.

METHODS

The Amazon Basin provides an ideal opportunity to evaluate the relationship between sediment supply, meander migration, and sinuosity adjustment over a large range of scales in the absence of engineering influences on channel mobility. The physiography of the basin leads to systematically varying sediment supplies throughout the drainage network, at least as measured in total suspended sediment fluxes (Guyot et al., 1989, 1994; Latrubesse et al., 2005; Filizola and Guyot, 2009). We selected 16 meandering reaches for study, sampling across the physiographic provinces of the Amazon (Fig. 1A; Table DR1 in the GSA Data Repository[1]). We ensured that the reaches had wide valley margins and were free from visible evidence of confining elements (e.g., bedrock exposures) as discerned from satellite imagery, although we have no way of assessing subtler erodibility differences in alluvium of the kind referred to by Schwendel et al. (2015), which

*E-mail: geomorphicjosh@gmail.com

[1]GSA Data Repository item 2019289, extended methods, Figures DR1–DR3, and Tables DR1–DR6, is available online at http://www.geosociety.org/datarepository/2019/, or on request from editing@geosociety.org.

CITATION: Ahmed, J., Constantine, J.A., and Dunne, T., 2019, The role of sediment supply in the adjustment of channel sinuosity across the Amazon Basin: Geology, https://doi.org/10.1130/G46319.1

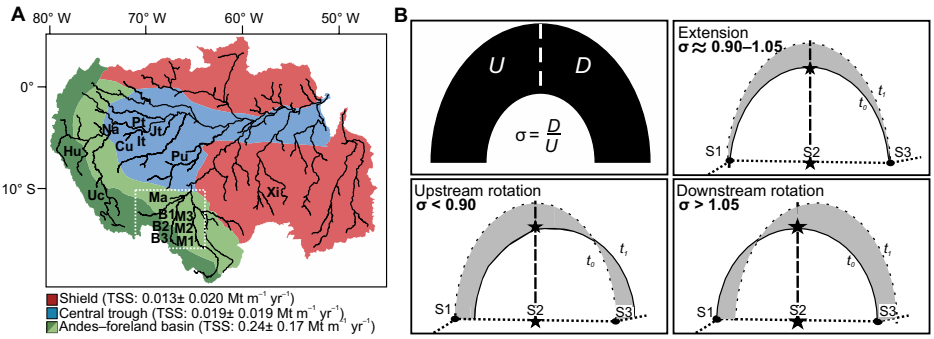

Figure 1. A: Amazon drainage basin symbolized by physiographic province and labeled with reach abbreviations: Xi—Xingu; Pu—Purus; Jt—Jutai; It—Ituí; Cu—Curuca; Pt—Putumayo; Na—Nanay; Hu—Huallaga; Uc—Ucayali; B1, B2, B3—Beni; M1, M2, M3—Mamoré; Ma—Madre de Díos. Exact reach coordinates can be found in Table DR1 (see footnote 1). Average annual width-normalized total suspended sediment flux (TSS, in megatons per meter of river channel width per year) values for each physiographic province are indicated; further information on their collection and representation can be found in the Data Repository. Dashed white box indicates reaches (excluding M3) resolved by near-annual imagery; remaining reaches are resolved at near decadal time scales. B: Meander symmetry index (σ) and exemplary scenarios. Clockwise from top left: σ is ratio of total eroded area produced between first (t_0) and final year (t_1) of record in downstream (*D*) versus upstream portions (*U*) of meander. Each meander is divided through bend apex as characterized by point of maximum curvature (star-ended vertical dashed line) of earliest centerline (t_0), and erosional areas are bounded by inflection points (curvature minimum) derived from connected reach segments (S1, S2, etc.) along t_0 centerline. Extension occurs when ratio between down- and upstream eroded areas is within range 0.90 < σ < 1.05, downstream rotation is where ratio is >1.05, and upstream rotation is where ratio is <0.90.

are incorporated into our average effects. Total suspended sediment (TSS) flux data compiled from various sources by Constantine et al. (2014) were normalized by bankfull channel width, because wider channels can convey larger sediment loads, and used as a proxy for the bed material supply to each reach, which was necessary in the absence of direct measurements of bed material flux (Table DR2).

Multispectral Landsat images from 1984 to 2014 were used to delineate bankfull channel margins. Reach imagery for three rivers (Mamoré, Beni, and Madre de Díos) was obtained at a near-annual resolution (Fig. 1A), while the remaining reaches had a temporal spacing of ~10 yr. The average bankfull channel width of each reach was measured along straight sections of river ($n > 20$ per reach). The bankfull channel boundary was delineated by selecting a representative pixel threshold at the channel-bank interface using the normalized difference vegetation index from composite images. The boundary was vectorized and used to generate centerlines for each year on record. After Micheli et al. (2004), overlapping centerlines between sequential time steps were then used to calculate reach-averaged channel migration rates (M_R), reported in units of channel widths per year.

The near-annual resolution of Landsat imagery available for the Mamoré, Beni, and Madre de Díos rivers allowed us to directly measure the fractional change in sinuosity resulting from channel migration (*S**) as the following:

$$S^* = \frac{1}{S_1}\left(\frac{S_2 - S_1}{t_2 - t_1}\right), \quad (1)$$

where S_1 and S_2 are channel sinuosity at the first and second time steps, measured as the ratio of reach length to valley length, and t is time. For the decadal data set where cutoffs were unavoidable, we determined *S** using a modified relation derived by Constantine and Dunne (2008, their equation 4), in which:

$$S^* = M^* + \frac{fL}{M_1}\frac{\Delta n}{\Delta t}, \quad (2)$$

where *M** is the fractional change in channel length measured directly from imagery between time steps, f is the fractional change in channel length resulting from meander cutoff, L is the characteristic length of a cutoff event in channel-width units, M_1 is the reach length at the first time step in channel-width units, and n is the number of cutoff events between time steps. Equation 2 was solved using information derived from our Landsat imagery (Table DR3) and from Constantine and Dunne (2008).

We developed a meander symmetry index (σ) to ensure a quantitative and repeatable method for describing the direction of planform geometry change resulting from meander migration (Fig. 1B). A symmetry index was calculated for each meander as defined by the ratio of the eroded areas created in the upstream versus downstream portions of the meander (see the methods in the Data Repository). Large σ values are indicative of downstream rotation, while small values describe more extensional or upstream bend deformation. In total, 281 measurements were made of reach-averaged channel migration rate (M_R) and *S**, while 16 measurements of σ were formed from reach-median values of individual σ measurements. We selected the reach-median metric to capture broad-scale meandering behavior that would otherwise be obscured by inter-meander variability.

RESULTS AND DISCUSSION

Fractional change in sinuosity resulting from channel migration (*S**) increases for rivers with greater rates of sediment supply, a pattern that is consistent for both the annual and decadal data sets (Fig. 2A). Rivers with TSS fluxes >0.05 Mt m^{-1} yr^{-1} increase their sinuosity significantly more rapidly than those with lower sediment loads. This relationship suggests that rivers characterized by high TSS fluxes undergo more rapid meander migration and sinuosity increase (Fig. 2B).

Reach-median σ indices positively correlate with increasing sediment load (Fig. 3A). Median σ values range from 0.95 to 3.25 (with variability described by the interquartile range [IQR] 0.50–2.46) for the decadal data, and from 1.39 to 3.55 (IQR 0.43–3.81) for the annual data (Table DR4). *S** is positively correlated with differences in meander deformation style (Fig. 3B), with rivers characterized by σ >1.50 experiencing, on average, more than four times greater sinuosity change than rivers where σ <1.50. Frequency distributions of σ values for each reach (Fig. DR1 in the Data Repository) illustrate that most meanders (36%–76%) rotated downstream (1.05 < σ < 5.0). The percentage of meanders with symmetry indices >5.0 increased for sediment-rich rivers in the basin, with up to 14% of their meanders having indices between 10.0 and 15.0. Although median values are all >1.0, a fraction of meanders within each reach (14%–47%) exhibit σ values <0.90, reflecting upvalley meander migration. Most upstream-rotating meanders are in reaches with moderate (<0.035 Mt m^{-1} yr^{-1}) sediment loads (Fig. DR1; Table DR2). Extensional meanders are consistently rare, comprising only 5%–24% of meanders across all reaches. In three sediment-rich reaches (M1, Hu, and Uc; Fig. 1A), 18%–24% of the meanders are extensional, which may be explained by the large number of temporally clustered cutoff events (2–13), which reduces the population of mature asymmetrical meanders on the reach.

Our results suggest a link between sediment supply and meander deformation, driven by sediment sequestration on point bars. Bar growth augments the curvature-driven components of the force balance driving sediment transport and bank erosion (Dietrich and Smith, 1983). Rivers with greater sediment loads can deposit this material as water shoals over the point bar and momentum diminishes in the lee, or as material is transported across the channel by transverse near-bed currents (Dietrich and Smith, 1984; Frothingham and Rhoads, 2003). Experimental evidence suggests that point bars grow preferentially in the downstream direction as sediment is deposited

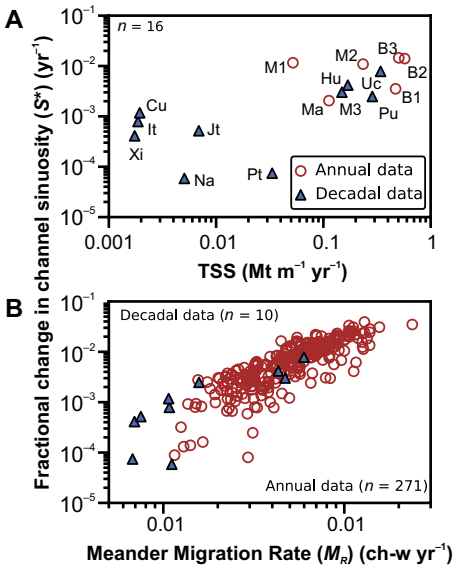

Figure 2. A: Width-normalized total suspended sediment flux (TSS, in megatons per meter of channel width per year) plotted against fractional change in channel sinuosity (*S, per year). Solid triangles represent decadal data set, while open circles represent temporally averaged data points from annually resolved data set. Reach names are labeled according to abbreviations in Figure 1A. B: Average annual channel migration rate (M_R, in channel widths [ch-w] per year) related to fractional change in channel sinuosity through time (*S**, per year). Solid triangles are derived from decadally resolved data set, and open circles indicate *S** values calculated for rivers from annually resolved data set. Statistical characteristics have been withheld from the figures, but are available in Table DR6 in the Data Repository (see footnote 1).**

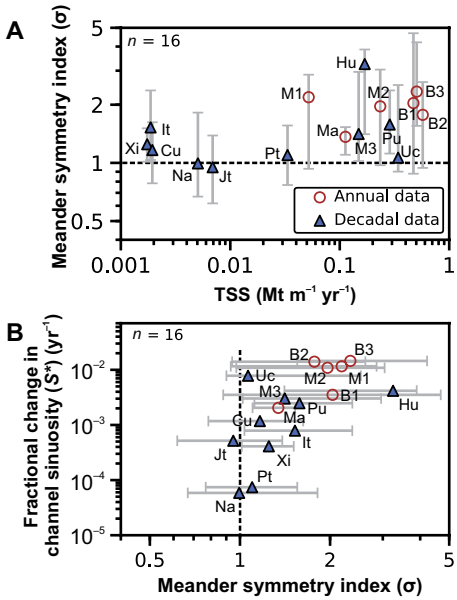

Figure 3. A: Width-normalized total suspended sediment load (TSS) plotted against reach-averaged meander symmetry index (σ). Dashed black line partitions data at extensional meander threshold (σ ≈ 1). Bars indicate statistical dispersion represented by interquartile range of symmetry indices for meanders on each reach. Solid triangles represent decadal data set, while open circles represent annual data set. B: Reach-averaged meander symmetry index (σ) plotted against fractional change in channel sinuosity (*S). Reaches are labeled according to abbreviations in Figure 1A.**

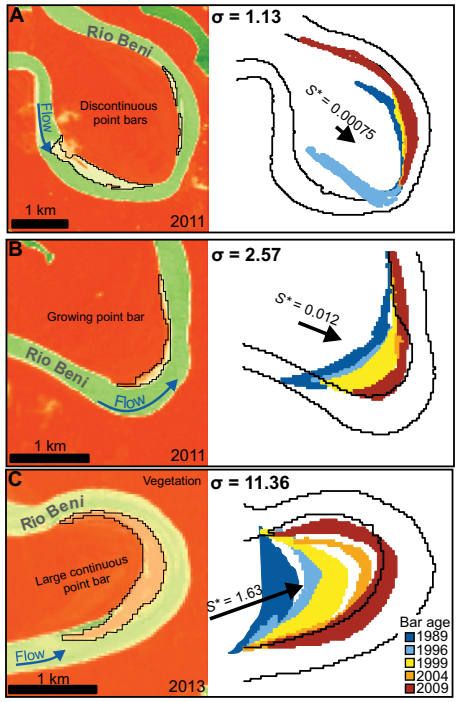

Figure 4. Meander deformation and point bar extents for three meanders on Beni River. On left, subaerial point bar extents are outlined in black on Landsat imagery converted to display normalized difference vegetation index (NDVI). On right, extents of point bars in five discrete years are displayed after extraction from Landsat imagery; warmer colors indicate younger deposits. Flow direction, meander symmetry indices (σ), and direction of bend movement are all annotated. Direction of movement was determined by visually inspecting bend for approximate trajectory between images. Each bend is prescribed a fractional change in sinuosity (*S) value calculated using the regression equation generated by fitting a power function ($S^* = 0.0005\sigma^{3.33}$) to the data in Figure 3B; associated arrows indicate rates of channel lengthening. Bar areas and meander locations are specified in Table DR5 in the Data Repository (see footnote 1).**

at the tail or on the margins of the bar (Dietrich et al., 1979; Pyrce and Ashmore, 2005; Braudrick et al., 2009). Frequent deposition associated with greater sediment fluxes should result in faster outward and downstream bar growth, enhancing the displacement and retention of high-velocity flows near the outer bank downstream of the meander apex. Downstream-rotational meanders experience more-sustained curvature-driven transfer of momentum to the outer bank and have well developed secondary circulation cells that facilitate the growth of longer, more developed point bars that begin at the upstream inflection (Abad and Garcia, 2009a, 2009b).

Upstream-rotating meanders were observed in all reaches and were especially common in reaches with low sediment loads. Although reported less frequently in the literature, upstream-rotating meanders have been previously documented (e.g., Seminara et al., 2001; Duan and Julien, 2010). Upstream rotation has been attributed to spatial variations in the erodibility of bank materials (Posner and Duan, 2012; Schwendel et al., 2015), to backwater effects caused by meander cutoff (Schwenk and Foufoula-Georgiou, 2017), and to the upstream valley orientation of tightly curved meanders (Abad and Garcia, 2009b). The role of low sediment supply and potentially slow bar growth in the initiation of upstream rotation requires further examination. However, our observations suggest that upstream-rotating meanders are associated with compound bend development or with sediment deposition at the bar head (Fig. DR2). Protruding sediment lobes are then generated that promote localized bank erosion upstream of the meander apex, similar to the observations of Nanson (1980) and Hagstrom et al. (2018).

We assessed the low-flow subaerial extent of point bars for three meanders on the Beni River (Fig. 4) to discern whether the direction of planform geometry change was related to systematic patterns of bar growth. In meanders with high σ values, bars tended to be longer, more continuous, and wider between inflection points. Conversely, extensional meanders had narrower, sometimes discontinuous, bars with smaller surface areas (Table DR5). Our observations are similar to those made in the laboratory experiments of Abad and Garcia (2009b), who observed larger, better-developed bar forms in downstream-rotational meanders. They attributed this development to the rapid cross-stream transition of the high-velocity core in response to the change in local curvature, which facilitated the development of stronger helical circulation cells and quicker establishment of the inner-bank bar.

Channel stability analysis suggests that in low-sinuosity rivers with poorly developed meanders, point bars are suppressed in favor of migrating alternate bars (Tubino and Seminara, 1990). In the Amazon Basin, this has been observed on rivers with low sediment supplies (e.g., Xingu River), while more sinuous channels (e.g., Beni River) are characterized by fixed point bars and high sediment loads (Monegaglia et al., 2017). Rivers enriched with sediment can construct point bars more rapidly, increasing bend length and channel curvature while facilitating channel migration. A positive feedback is initiated wherein greater sediment loads encourage bar growth and channel curvature, ultimately exceeding the curvature threshold required for the persistence of fixed point bars over migrating bars. Rivers in which meanders are unable to grow as quickly fail to attain the necessary curvature required to establish permanent fixed bars, therefore limiting sinuosity growth.

CONCLUSIONS

The direction of meander deformation determines how channel sinuosity evolves in response to meander migration. The fractional rate of sinuosity change is observed to vary as a function of sediment supply for a range of rivers across the Amazon Basin. This relationship between sinuosity change and sediment supply is manifested through the rate of alluvial sequestration onto point bars. Alluvium is typically sequestered downstream of the bar apex, facilitating the down-channel growth of the bar. For upstream-rotating meanders, sediment accumulates near the head of the bar, creating lobes that protrude into the channel, locally increasing curvature and inducing bank erosion upstream of the meander apex. Extensional meanders are rare, reflecting an early stage of meander development. The meander symmetry index, which quantifies the geometric change in meander growth, is also correlated with sediment supply and rates of channel growth. Our results suggest that the evolution of meandering rivers is strongly tied to upstream supplies of sediment. These are responsible for the turnover of floodplain sediments, nutrients, and habitats and the creation and preservation of alluvial architecture important for recording the river's evolutionary history through time.

ACKNOWLEDGMENTS

We would like to thank Bodo Bookhagen for assistance with the development of channel extraction methodologies, Alex Horton for assistance with curvature data generation, Joan Teng for assistance with Landsat imagery collection, and Rolf Aalto for useful discussions relating to discharge variability. We also thank T.C. Hales and the reviewers for constructive comments that helped improve the clarity and quality of the manuscript .

REFERENCES CITED

Abad, J.D., and Garcia, M.H., 2009a, Experiments in a high-amplitude Kinoshita meandering channel: 1. Implications of bend orientation on mean and turbulent flow structure: Water Resources Research, v. 45, W02401, https://doi.org/10.1029/2008WR007016.

Abad, J.D., and Garcia, M.H., 2009b, Experiments in a high-amplitude Kinoshita meandering channel: 2. Implications of bend orientation on bed morphodynamics: Water Resources Research, v. 45, W02402, https://doi.org/10.1029/2008WR007017.

Braudrick, C.A., Dietrich, W.E., Leverich, G.T., and Sklar, L.S., 2009, Experimental evidence for the conditions necessary to sustain meandering in coarse-bedded rivers: Proceedings of the National Academy of Sciences of the United States of America, v. 106, p. 16,936–16,941, https://doi.org/10.1073/pnas.0909417106.

Bufe, A., Paola, C., and Burbank, D.W., 2016, Fluvial bevelling of topography controlled by lateral channel mobility and uplift rate: Nature Geoscience, v. 9, p. 706–710, https://doi.org/10.1038/ngeo2773.

Constantine, J.A., and Dunne, T., 2008, Meander cutoff and the controls on the production of oxbow lakes: Geology, v. 36, p. 23–26, https://doi.org/10.1130/G24130A.1.

Constantine, J.A., Dunne, T., Ahmed, J., Legleiter, C., and Lazarus, E.D., 2014, Sediment supply as a driver of river meandering and floodplain evolution in the Amazon Basin: Nature Geoscience, v. 7, p. 899–903, https://doi.org/10.1038/ngeo2282.

Dietrich, W.E., and Smith, J.D., 1983, Influence of the point bar on flow through curved channels: Water Resources Research, v. 19, p. 1173–1192, https://doi.org/10.1029/WR019i005p01173.

Dietrich, W.E., and Smith, J.D., 1984, Bed load transport in a river meander: Water Resources Research, v. 20, p. 1355–1380, https://doi.org/10.1029/WR020i010p01355.

Dietrich, W.E., Smith, J.D., and Dunne, T., 1979, Flow and sediment transport in a sand bedded meander: The Journal of Geology, v. 87, p. 305–315, https://doi.org/10.1086/628419.

Duan, J.G., and Julien, P.Y., 2010, Numerical simulation of meandering evolution: Journal of Hydrology (Amsterdam), v. 391, p. 34–46, https://doi.org/10.1016/j.jhydrol.2010.07.005.

Dunne, T., Constantine, J.A., and Singer, M.B., 2010, The role of sediment transport and sediment supply in the evolution of river channel and floodplain complexity: Transactions of the Japanese Geomorphological Union, v. 31, p. 155–170, http://ci.nii.ac.jp/naid/110007621738/en/.

Filizola, N., and Guyot, J.L., 2009, Suspended sediment yields in the Amazon basin: An assessment using the Brazilian national data set: Hydrological Processes, v. 23, p. 3207–3215, https://doi.org/10.1002/hyp.7394.

Frothingham, K.M., and Rhoads, B.L., 2003, Three-dimensional flow structure and channel change in an asymmetrical compound meander loop, Embarras River, Illinois: Earth Surface Processes and Landforms, v. 28, p. 625–644, https://doi.org/10.1002/esp.471.

Guyot, J.L., Bourges, J., Calle, H., Cortes, J., Hoorelbecke, R., and Roche, M.A., 1989, Transport of suspended sediments to the Amazon by an Andean river: The river Mamore, Bolivia, *in* Proceedings of the Fourth International Symposium on River Sedimentation, June 5–9, 1989: Beijing, China Ocean Press, v. 1.

Guyot, J.L., Bourges, J., and Cortez, J., 1994, Sediment transport in the Rio Grande, an Andean river of the Bolivian Amazon drainage basin, *in* Olive, L.J., et al., eds., Variability in Stream Erosion and Sediment Transport: International Association of Hydrological Sciences Series of Proceedings and Reports 224, p. 223–231.

Hagstrom, C.A., Leckie, D.A., and Smith, M.G., 2018, Point bar sedimentation and erosion produced by an extreme flood in a sand and gravel-bed meandering river: Sedimentary Geology, v. 377, p. 1–16, https://doi.org/10.1016/j.sedgeo.2018.09.003.

Hickin, E.J., and Nanson, G.C., 1975, The character of channel migration on the Beatton River, northeast British Columbia, Canada: Geological Society of America Bulletin, v. 86, p. 487–494, https://doi.org/10.1130/0016-7606(1975)86<487:TCOCMO>2.0.CO;2.

Hooke, J.M., 1984, Changes in river meanders: Progress in Physical Geography, v. 8, p. 473–508, https://doi.org/10.1177/030913338400800401.

Latrubesse, E.M., Stevaux, J.C., and Sinha, R., 2005, Tropical rivers: Geomorphology, v. 70, p. 187–206, https://doi.org/10.1016/j.geomorph.2005.02.005.

Legleiter, C.J., Harrison, L.R., and Dunne, T., 2011, Effect of point bar development on the local force balance governing flow in a simple, meandering gravel bed river: Journal of Geophysical Research: Earth Surface, v. 116, F01005, https://doi.org/10.1029/2010jf001838.

Lewin, J., 1976, Initiation of bed forms and meanders in coarse-grained sediment: Geological Society of America Bulletin, v. 87, p. 281–285, https://doi.org/10.1130/0016-7606(1976)87<281:IOBFAM>2.0.CO;2.

Micheli, E.R., Kirchner, J.W., and Larsen, E.W., 2004, Quantifying the effect of riparian forest versus agricultural vegetation on river meander migration rates, central Sacramento River, California, USA: River Research and Applications, v. 20, p. 537–548, https://doi.org/10.1002/rra.756.

Monegaglia, F., Tubino, M., and Zolezzi, G., 2017, Dynamics of migrating alternate bars in large meandering rivers: Combining remote sensing and theoretical approaches, *in* Lanzoni, S., et al., eds., RCEM2017—Back to Italy: The 10th Symposium on River, Coastal, and Esuarine Morphodynamics—Book of Abstracts: Trento-Padova, Italy, RCEM2017 Organizing Committee, p. 66.

Nanson, G.C., 1980, Point bar and floodplain formation of the meandering Beatton River, northeastern British Columbia, Canada: Sedimentology, v. 27, p. 3–29, https://doi.org/10.1111/j.1365-3091.1980.tb01155.x.

Ouchi, S., 1985, Response of alluvial rivers to slow active tectonic movement: Geological Society of America Bulletin, v. 96, p. 504–515, https://doi.org/10.1130/0016-7606(1985)96<504:ROARTS>2.0.CO;2.

Posner, A.J., and Duan, J.G., 2012, Simulating river meandering processes using stochastic bank erosion coefficient: Geomorphology, v. 163–164, p. 26–36, https://doi.org/10.1016/j.geomorph.2011.05.025.

Pyrce, R.S., and Ashmore, P.E., 2005, Bedload path length and point bar development in gravel-bed river models: Sedimentology, v. 52, p. 839–857, https://doi.org/10.1111/j.1365-3091.2005.00714.x.

Schumm, S.A., and Khan, H.R., 1972, Experimental study of channel patterns: Geological Society of America Bulletin, v. 83, p. 1755–1770 https://doi.org/10.1130/0016-7606(1972)83[1755:ESOCP]2.0.CO;2.

Schuurman, F., Shimizu, Y., Iwasaki, T., and Kleinhans, M.G., 2016, Dynamic meandering in response to upstream perturbations and floodplain formation: Geomorphology, v. 253, p. 94–109, https://doi.org/10.1016/j.geomorph.2015.05.039.

Schwendel, A.C., Nicholas, A.P., Aalto, R.E., Sambrook Smith, G.H., and Buckley, S., 2015, Interaction between meander dynamics and floodplain heterogeneity in a large tropical sand-bed river: The Rio Beni, Bolivian Amazon: Earth Surface Processes and Landforms, v. 40, p. 2026–2040, https://doi.org/10.1002/esp.3777.

Schwenk, J., and Foufoula-Georgiou, E., 2017, Are process nonlinearities encoded in meandering river planform morphology?: Journal of Geophysical Research: Earth Surface, v. 122, p. 1534–1552, https://doi.org/10.1002/2016JF003929.

Seminara, G., Zolezzi, G., Tubino, M., and Zardi, D., 2001, Downstream and upstream influence in river meandering. Part 2. Planimetric development: Journal of Fluid Mechanics, v. 438, p. 213–230, https://doi.org/10.1017/S0022112001004281.

Tal, M., and Paola, C., 2007, Dynamic single-thread channels maintained by the interaction of flow and vegetation: Geology, v. 35, p. 347–350, https://doi.org/10.1130/G23260A.1.

Tubino, M., and Seminara, G., 1990, Free-forced interactions in developing meanders and suppression of free bars: Journal of Fluid Mechanics, v. 214, p. 131–159, https://doi.org/10.1017/S0022112090000088.

Printed in USA